

# Impact of Lake/reservoir Expansion and Shrinkage on Energy and Water Vapor Fluxes in the Surrounding Area

Shaomin Liu<sup>1</sup>, Ailun Guo<sup>2</sup>, Zhongli Zhu<sup>3</sup>, Ziwei Xu<sup>1</sup>, Qing Xiao<sup>4</sup>, Qian Ju<sup>1</sup>, Yuan Zhang<sup>1</sup>, and Xiaofan Yang<sup>1</sup>

<sup>1</sup>Beijing Normal University

<sup>2</sup>Peking University

<sup>3</sup>School of Geography, Beijing Normal University

<sup>4</sup>Institute of Remote Sensing and Digital Earth

November 24, 2022

## Abstract

Lakes and reservoirs are important components of freshwater. The expansion and shrinkage of lakes/reservoirs may alter meteorological characteristics and the underlying surface conditions, which would further affect energy and water vapor fluxes in the surrounding area. In this study, the expansion and shrinkage of the Guanting Reservoir during 2013-2017 was analyzed using remote sensing data. Data collected from the Huailai Remote Sensing Experiment Station were used to analyze the energy and water vapor fluxes. The results showed the annual expansion of the Guanting Reservoir from 2013 to 2017, and a seasonal variation characterized by expansion in spring, shrinkage in summer and autumn, and expansion again in winter was exhibited. Meanwhile, the evapotranspiration (ET) in the surrounding area also increased annually. In the growing season, the seasonal shrinkage of the reservoir indirectly affected ET through net radiation, deep soil moisture and vegetation growth conditions, while in the non-growing season, the seasonal expansion directly increased ET by increasing the proportion of water bodies in the source area and increased net radiation and surface soil moisture. In addition, with the reservoir expanding year by year, the difference in ET between the closer site and further site from the reservoir increased obviously, especially in the non-growing season during the seasonal expansion of the reservoir. The results help with the ecosystem restoration and sustainable development of lakes/reservoirs in arid and semiarid areas.



21 **Abstract:**

22 Lakes and reservoirs are important components of freshwater. The expansion and shrinkage of  
23 lakes/reservoirs may alter meteorological characteristics and the underlying surface conditions,  
24 which would further affect energy and water vapor fluxes in the surrounding area. In this study,  
25 the expansion and shrinkage of the Guanting Reservoir during 2013-2017 was analyzed using  
26 remote sensing data. Data collected from the Huailai Remote Sensing Experiment Station were  
27 used to analyze the energy and water vapor fluxes. The results showed the annual expansion of  
28 the Guanting Reservoir from 2013 to 2017, and a seasonal variation characterized by expansion  
29 in spring, shrinkage in summer and autumn, and expansion again in winter was exhibited.  
30 Meanwhile, the evapotranspiration (ET) in the surrounding area also increased annually. In the  
31 growing season, the seasonal shrinkage of the reservoir indirectly affected ET through net  
32 radiation, deep soil moisture and vegetation growth conditions, while in the non-growing season,  
33 the seasonal expansion directly increased ET by increasing the proportion of water bodies in the  
34 source area and increased net radiation and surface soil moisture. In addition, with the reservoir  
35 expanding year by year, the difference in ET between the closer site and further site from the  
36 reservoir increased obviously, especially in the non-growing season during the seasonal  
37 expansion of the reservoir. The results help with the ecosystem restoration and sustainable  
38 development of lakes/reservoirs in arid and semiarid areas.

39

## 40 **1. Introduction**

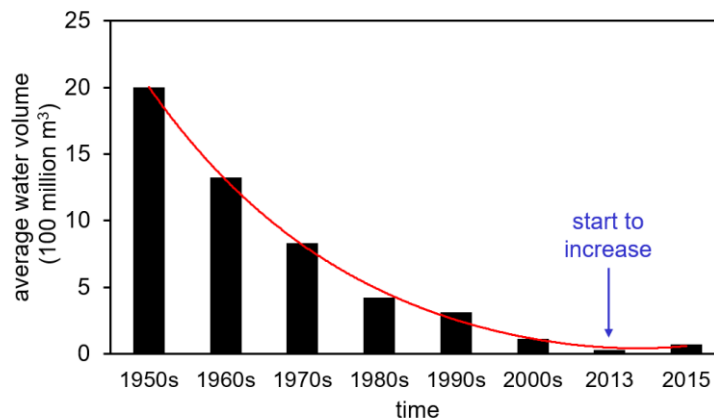
41 Lakes and reservoirs only occupy approximately 4% of the global terrestrial surface  
42 (Downing et al. 2006), but they are of great importance due to their significant contributions to  
43 the water supply (Lee et al. 2014). In arid and semiarid regions of China, lakes and reservoirs  
44 provide major freshwater resources for inland watersheds and basins. Previous studies have  
45 indicated that the expansion and shrinkage of lakes/reservoirs are not only caused by climate  
46 change (Williamson et al., 2009; Xiao et al., 2018) but also by human activities (e.g., agricultural  
47 irrigation, dam construction and water conservancy projects) (Guo et al., 2008, 2012; Shi et al.  
48 2012; Ruan et al., 2012; Haddeland et al. 2014; Shadkam et al., 2016; Xie et al., 2017). In turn,  
49 the expansion and shrinkage of lakes/reservoirs would also have an impact on the local  
50 microclimate and thus affect crop yields and agricultural development in the surrounding areas  
51 (Min et al., 1995).

52 The lake effect is a function of the climatic conditions in which a lake is situated, the local  
53 setting of the lake and its surroundings and the morphometry of the lake itself (Kodama et al.,  
54 1983). Since lakes/reservoirs act differently than surrounding lands in the exchanges of radiation  
55 and energy and water vapor, these water bodies influence local, regional and even global  
56 climates (Bates et al., 1993; Rouse et al., 2005; Liu et al., 2012; Biermann et al., 2014; Li et al.,  
57 2016). For example, the lake effect of Lake Minchumina led to a longer growing season than  
58 other stations in interior Alaska, which showed the lake's warming effect in the surrounding  
59 areas (Kodama et al., 1983). Additionally, the large thermal contrast between lakes/reservoirs  
60 and their surrounding lands often triggers thermal circulation, which has a significant impact on  
61 energy and water vapor transport (Lee, et al., 2014).

62 Currently, hydrometeorological observations are obtained to measure surface energy and  
63 water vapor fluxes, and these measurement devices include lysimeters, the Bowen ratio energy  
64 balance system, the eddy covariance system (EC), scintillometers, and so on (Liu et al., 2013).  
65 However, long-term (>1 yr) measurements of surface energy and water vapor fluxes for  
66 lake/reservoir systems have remained challenging until recently (Liu et al., 2012; Lee et al.  
67 2014). In recent years, through direct observations of energy and water vapor fluxes on  
68 lakes/reservoirs, previous studies have analyzed the characteristics of water-atmosphere  
69 interactions on lakes/reservoirs, including the surface energy budget (Li et al., 2016), carbon  
70 cycle (Vesala et al., 2006), and energy balance closure (Nordbo et al., 2011; Wang et al., 2017).  
71 Furthermore, the energy and water vapor fluxes of two kinds of underlying surfaces, water and  
72 land surfaces, have been compared, including lake/desert, lake/forest, and lake/farmland surfaces  
73 (Liu et al., 2008). For example, using the EC technique, the latent and sensible heat fluxes from  
74 lake and forest surfaces were compared in two lakes in central Sweden (Venäläinen et al., 1998),  
75 as well as in Lake Valkea-Kotinen in southern Finland (Vasala et al., 2006; Nordbo et al., 2011).  
76 The differences between the meteorological characteristics (such as energy distribution and  
77 turbulence intensity) of lake and desert surfaces were also analyzed in the Badan Jaran Desert  
78 (Ma et al., 2012; Ao et al., 2013; Zhang et al., 2014). However, these studies analyzed the energy  
79 and water vapor fluxes over either water or land surfaces, rather missing the interactions between  
80 the lake/reservoir and land surfaces.

81 In arid and semiarid areas with less precipitation and little vegetation in China, human  
82 activities play a dominant role in the expansion and shrinkage of lakes/reservoirs. Guanting  
83 Reservoir is located in Huailai County, Hebei Province, China, adjacent to Beijing, which  
84 belongs to the semiarid area in the North China Plain (NCP). After its construction in 1954, the

85 Guanting Reservoir was seriously contaminated by industrial waste, and the water volume of the  
86 reservoir continued to decline until 2013 (Yang et al., 2016) (Figure 1), which was mainly  
87 caused by the increasing agricultural water consumption and hydraulic projects occurring in the  
88 upstream areas (Chen, 2007). In recent years, in preparation for the 24th Winter Olympic Games  
89 in Beijing, the government enforced environmental protection strategies and policies, which  
90 were expected to improve the water quality and water level of the Guanting Reservoir. This  
91 study aimed to analyze the responses of energy and water vapor fluxes to the expansion and  
92 shrinkage of lakes/reservoirs. First, remote sensing data were used to analyze the interannual and  
93 seasonal expansion and shrinkage of the Guanting Reservoir. Second, long-term large-aperture  
94 scintillometer (LAS) and automatic weather station (AWS) data were used to analyze the  
95 relationship between the expansion and shrinkage of the reservoir and the variations in energy  
96 and water vapor fluxes in surrounding areas. Finally, using EC and AWS data from two nearby  
97 observational sites, the variations in energy and water vapor fluxes at different distances from the  
98 reservoir were analyzed, and the influencing mechanism was discussed. This study also provides  
99 scientific implications for the ecosystem restoration and sustainable development of  
100 lakes/reservoirs in arid and semiarid areas.



101

102 Figure 1. Variations in the water volume in the Guanting Reservoir from the 1950s to 2015 (the water  
103 volume data were adopted from Yang et al., 2015 and Chen et al., 2007).

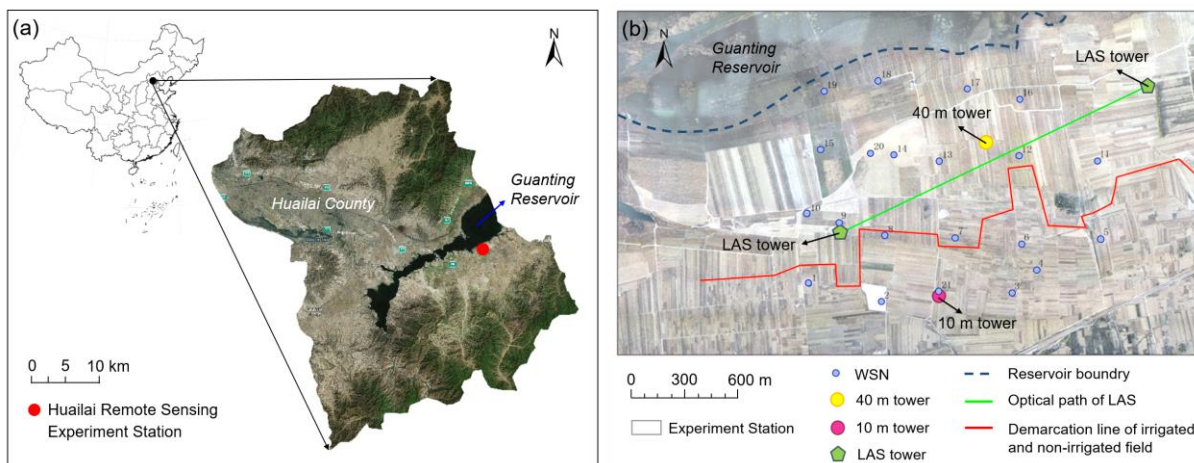
## 104 **2. Materials and Methods**

### 105 **2.1 Site Description and Measurements**

106 The study area is on the southeastern shore of the Guanting Reservoir, which is in the  
107 middle reaches of the Hai River Basin. The study site was located in the Huailai Remote Sensing  
108 Experiment Station (latitude 40° 20' N, longitude 115° 47' E, Figure 2a), Hebei Province, China.  
109 The station is in the southwest area of the Yanqing-Huailai Basin, and on its north and south  
110 sides are northwest- to southeast-trending mountains. The climate is described as a temperate  
111 continental monsoon climate. The mean temperature is approximately 10.1 °C, the maximum  
112 temperature in summer is approximately 39 °C, and the minimum temperature in winter is below  
113 -20 °C. The mean annual precipitation is approximately 370 mm, which is mainly concentrated  
114 in summer. The annual average wind speed is 3.4 m·s<sup>-1</sup>. The prevailing wind direction is west in  
115 winter and early spring, and it is southeast in summer and autumn (Yang et al., 2015). The soils  
116 in the study area are sandy alluvial soil, and the main crops are single-season maize, which is  
117 planted in early May and matures in mid-to-late September each year (Yang et al., 2015).

118 The experimental area has a range of approximately 2 km×1 km, which can be divided into  
119 irrigated and non-irrigated farmland and is shown bounded by the red lines in Figure 2b. The 10  
120 m tower was on irrigated farmland, and the 40 m tower was on non-irrigated farmland. The  
121 observation variables used in this study and their configuration information are shown in Table  
122 1. Specifically, a group of LASs, two sets with the transmitter and receiver exchanged for each  
123 other was installed in the northeast-southwest direction, and the field of view of the instruments,  
124 which can be defined by the source area (Liu et al., 2013), includes both irrigated and non-

125 irrigated fields. Two ECs and two AWSs were installed on both the 10 m and 40 m towers to  
 126 observe sensible heat flux (H), latent heat flux (LE), and meteorological elements (including  
 127 four-component radiation, precipitation, wind speed/direction, air temperature/humidity, soil  
 128 temperature/moisture profile, and so on). In addition, seven layers of meteorological gradient  
 129 observation systems were installed at the 40 m tower.



130  
 131 Figure 2. The Huailai Remote Sensing Experiment Station: (a) The location of the Huailai Remote  
 132 Sensing Experiment Station, and (b) the observation system of the Huailai Experiment Station that was  
 133 used in this study (the background image is the image of the surrounding area of the reservoir in 2013).

134 The south side of the red line is the irrigated field, and the north side is the non-irrigated field.

135 Table 1. The observation instrument of the Huailai Experiment Station used in this study

Instrument	Variable	Site	Sensor Type	Height/Depth (m)
LAS	Sensible heat flux ( $W m^{-2}$ )	14m transmitting and receiving LAS tower	BLS450, Scintec, Germany; RR-RSS460, China	14 (path length: 1870m)
EC	Sensible heat flux and latent heat flux	on 10m tower	CSAT3&Li7500A, Campbell/Li-cor, USA	5

	(W m <sup>-2</sup> )	on 40m tower	CSAT3&EC150, Campbell, USA	3.5
AWS	Air	on 10m tower	HMP45C, Vaisala, Finland	5
	temperature/humidity (°C, %)	on 40m tower	HMP155A, Vaisala, Finland	3,5,10,15,20,30,40
	Wind speed/direction (m s <sup>-1</sup> , °)	on 10m tower	Ws03001, RM Young, USA	10
		on 40m tower	010C/020C, Met One, USA	3,5,10,15,20,30,40
	Soil heat flux (W m <sup>-2</sup> )	1.5m from 10m tower	HFT3, Campbell, USA	0. 06
		3m from 40m tower	HFP01, Hukseflux, Netherland	0. 06
	Soil temperature/moisture profile (°C, %)	1.5m from 10m tower	AV-10TH, Avalon, USA ECH <sub>2</sub> O-5, Decagon Devices, USA	0.02,0.04,0.10,0.2 0, 0.40,0.80,1.20,1.6 0
		3m from 40m tower	109 CS616, Campbell, USA	0.02,0.04,0.10,0.2 0, 0.40,0.80,1.20,1.6 0
	Air pressure (hpa)	on 10m/40m tower	PTB110, Vaisala, Finland	5/10
	Precipitation (mm)	on 10m tower	TE525MM, Campbell, USA	10

	on 40m tower	TE525MM, Campbell, USA	2.8
Four-component radiation (W m <sup>-2</sup> )	on 10m tower	CNR4, Kipp&Zonen, Netherland	5
	on 40m tower	CNR4, Kipp&Zonen, Netherland	4

## 136 2.2 Data Processing

137 Careful data processing and quality assessment are important to ensure the accuracy of the  
 138 observation data and are critical for obtaining reliable results.

### 139 2.2.1 Flux and Meteorological Data

140 The LAS is a device that derives the turbulence intensity by measuring the refractive index  
 141 of air ( $C_n^2$ ) (Wang et al., 1978). Data were carefully screened to ensure the data quality of LAS  
 142 observations, including [1] the exclusion of unreasonable data from raw  $C_n^2$  data, [2] rejection of  
 143  $C_n^2$  beyond the saturation criterion, [3] rejection of data with weak demodulated signals, and [4]  
 144 rejection of data during periods of precipitation. Then, the sensible heat flux was iteratively  
 145 calculated by combining meteorological data based on the Monin-Obukhov similarity theory  
 146 (Liu et al., 2013). After the sensible heat flux was obtained, the latent heat flux/ET could be  
 147 estimated from the energy balance equation, where the radiation and soil heat fluxes are the  
 148 mean results at the two observation sites. There are two LAS set observations (BLS450 and RR-  
 149 RSS460 obtained by Germany and China, respectively), and the data were primarily obtained  
 150 from the BLS450 measurements; missing flux measurements from BLS450 were filled with  
 151 measurements from RR-RSS460. A nonlinear regression method was used to fill the gaps to  
 152 obtain the continuous ET.

153 The software Eddypro (LI-COR Company,  
154 [https://www.licor.com/env/products/eddy\\_covariance/software.html](https://www.licor.com/env/products/eddy_covariance/software.html)) is used to process the EC  
155 data from 10 Hz, including spike removal, lag correction, performance of the planar fit  
156 coordinate rotation, frequency response correction, and so on. The EC data were averaged over  
157 30-min periods and then screened (Li et al., 2018). In addition, the 30-min data were also filtered  
158 in a four-step procedure: [1] data from periods of sensor malfunction were rejected, [2]  
159 incomplete 30-min data were rejected when the missing data constituted more than 10% of the  
160 raw data record, [3] data within 1 h before or after precipitation were rejected, and [4] data at  
161 night when the turbulence was weak ( $u^*$  less than 0.1 m/s) were rejected (Liu et al., 2011; Xu et  
162 al., 2013). To acquire the accumulative ET, the look-up table (LUT) method was used to fill the  
163 gaps, and the Bowen ratio closure method was used to force the energy balance (Liu et al.,  
164 2016).

165 The AWS data used in this study are listed in Table 1. In the data processing, data that are  
166 obviously beyond the range of physical possibilities are rejected, and the gaps are filled by the  
167 linear interpolation method (Jia et al., 2012). The soil heat flux plates at the 10 m and 40 m  
168 towers were buried at depths of 0.06 m, where one was buried in a maize field (G1), and the  
169 other two were buried in the soil surface (G2 and G3). The surface soil heat flux (G0) was  
170 calculated using the “PlateCal” approach (Liebethal et al., 2005) based on the combination of  
171 weighted vegetation fraction, soil temperature and moisture measured above the heat plates.

### 172 **2.2.2 Remote Sensing Data**

173 Landsat OLI (Operational Land Imager) data retrieved from the United States Geological  
174 Survey (USGS) website (<https://earthexplorer.usgs.gov/>) were used in this study, and the  
175 resolution was 30 m. We obtained 36 images in total, covering the Guanting Reservoir and its

176 surrounding area in 2013-2017. The data were corrected using ENVI 5.3 software, including  
177 cutting, radiometric calibration and FLAASH atmospheric correction. The normalized difference  
178 vegetation index (NDVI, with a resolution of 30 m) was calculated using the reflectance in the  
179 near-infrared ( $\rho_{\text{NIR}}$ ) and red bands ( $\rho_{\text{R}}$ ).

### 180 **2.2.2 Footprint Model**

181 The footprint is a function that describes the relationship between the spatial distribution of  
182 sources or sinks near the surface layer and the surface flux data measured by instruments, and the  
183 footprint can be estimated by the footprint model. The source area refers to the upwind area that  
184 has a major contribution to the flux observations and is the integral of the footprint function in a  
185 particular region. To estimate the flux footprint of EC, the method proposed by Kormann and  
186 Meixner (2001) was used, which is an Eulerian analytic flux footprint model (Liu et al., 2013).  
187 For LAS, the footprint can be described by a spatial weight function along its optical length,  
188 combining the footprint model for point fluxes with the path-weighting function of the LAS (Liu  
189 et al., 2011). In this study, we used daytime (6:00-22:00) footprints of EC and LAS during 2013-  
190 2017. The resolution of the source area was 30 m for both the EC and LAS measurements, and  
191 the flux contribution of the source area was set to 90%.

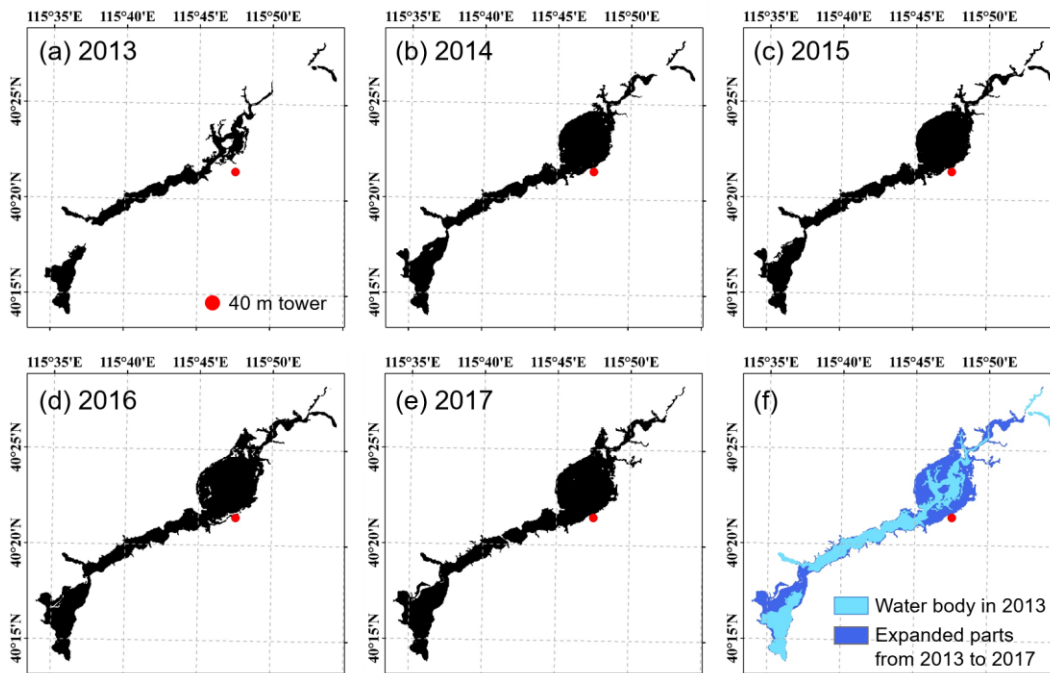
## 192 **3. Results and Discussion**

### 193 **3.1 Expansion and Shrinkage of the Guanting Reservoir**

194 The water areas on selected dates during the middle of the growing season (July to August)  
195 in 2013-2017 were used to analyze the interannual variations in expansion and shrinkage of the  
196 Guanting Reservoir, including 6 July 2013, 25 July 2014, 12 July 2015, 7 July 2016, and 17 July  
197 2017. Using the supervised classification method, the water areas in the last five years were

198 extracted, and the distances between the reservoir and observation point (40 m tower) were  
199 calculated.

200 Figure 3 shows the water area of the Guanting Reservoir, which shows that the reservoir  
201 expanded after 2013. The water bodies of the reservoir in 2013 and 2017 were compared in  
202 Figure 3f, which shows the overall variation. The northeastern part of the Guanting Reservoir  
203 had the most significant expansion over five years, and the Huailai Experimental Station is  
204 located in this area. This expansion in this area is because the topography of the northeast part of  
205 the reservoir is wide and flat, while the southwest part is narrow and deep. Under the same  
206 conditions of water volume change, the northeast part has the most significant expansion and  
207 shrinkage.



208  
209 Figure 3. The ranges of the Guanting Reservoir: (a) - (e) the water body ranges from 2013 to 2017, and (f)  
210 the comparison of the water body extents in 2013 and 2017.

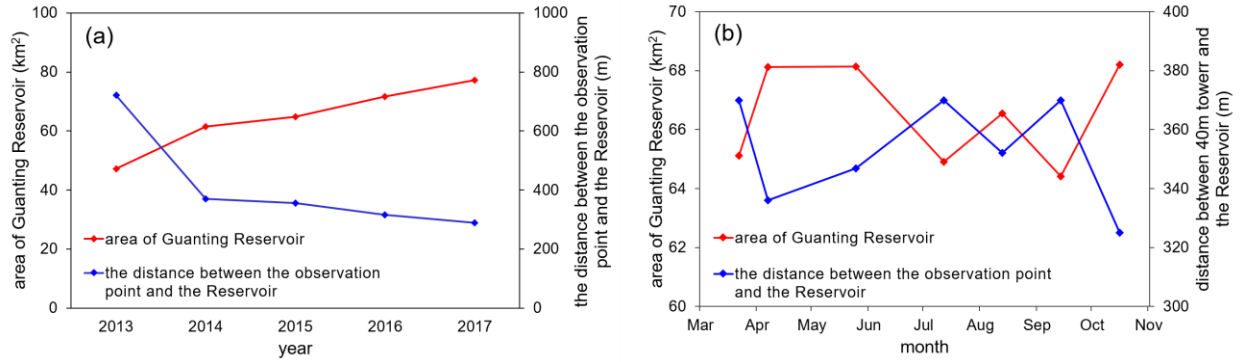
211 Figure 4a shows the variations in water area and the distances between the reservoir and  
212 observation points in 2013-2017. From 47.21 km<sup>2</sup> in 2013 to 77.25 km<sup>2</sup> in 2017, the water area  
213 of the Guanting Reservoir increased gradually and had a total increase of 63.63%. In addition,  
214 with the increase in reservoir area, the distance between the 40 m tower and the reservoir  
215 gradually decreased from 720.7 m in 2013 to 289.4 m in 2017, which decreased by  
216 approximately 430 m in five years.

217 The interannual expansion and shrinkage of the Guanting Reservoir was closely related to  
218 the large hydraulic projects built in the upstream and the large agricultural water with low water  
219 use efficiency (Yang et al., 2015). According to Ma et al. (2014), during 1978-2013, the water  
220 area change in the Guanting Reservoir was weakly correlated with natural factors, such as  
221 precipitation and air temperature but was significantly negatively correlated with regional gross  
222 national product (GNP), especially the gross domestic product (GDP) of secondary industry and  
223 was significantly positively correlated with cultivated area. Therefore, the expansion and  
224 shrinkage of the Guanting Reservoir was mainly influenced by human factors, especially the  
225 interception/discharge of the reservoirs and the irrigation water use in the upstream area. For  
226 example, in Figure 4a, 2013-2014 is the fastest stage of the expansion. In these two years, the  
227 area of cultivated land in the upstream did not change significantly, but in October 2013 in the  
228 historical data, the Youyi Reservoir in the upstream started to transfer water to the Guanting  
229 Reservoir to meet the water supply demand in Beijing. The total water discharge reached 15  
230 million m<sup>3</sup> (He et al., 2013), which directly led to the obvious expansion of the Guanting  
231 Reservoir in 2013-2014.

232 Since the distribution of precipitation is uneven during a year and the upstream water use  
233 changes seasonally, the area of the Guanting Reservoir also has seasonal variations. In this study,

234 we take 2015 as an example to analyze the seasonal variation in the expansion and shrinkage of  
235 the Guanting Reservoir. Seven images from March to October were used to extract the water  
236 body, including 22 March, 7 April, 25 May, 12 July, 13 August, 14 September and 16 October,  
237 and the distances between the 40 m tower and reservoir were calculated. The results are shown in  
238 Figure 4b. There was a rapid expansion from March to April, and then, the reservoir shrank from  
239 June to July and expanded again in October. In 2015, the maximum water area of the Guanting  
240 Reservoir appeared from April to May, with an area of approximately 68 km<sup>2</sup>; the minimum area  
241 of the reservoir occurred in September, which was approximately 64.4 km<sup>2</sup>, and the reservoir  
242 area changed by 3 km<sup>2</sup> during the year. The distance between the observation point and the  
243 reservoir decreased sharply during the spring; in 2015, the distance decreased from 370 m to 336  
244 m. From May to July, the distance increased gradually and reached its maximum, and in  
245 October, the distance decreased again and reached its minimum, which was approximately 325  
246 m in 2015. The distance between the observation point and the reservoir can be changed by  
247 approximately 45 m within a year.

248 In a year, the variations in irrigation water upstream of the Guanting Reservoir are closely  
249 related to the seasonal variation in the water area. The irrigation water was higher in the growing  
250 season (summer and autumn) and lower in the non-growing season (winter and spring).  
251 Therefore, the increase in irrigation water upstream made the Guanting Reservoir shrink, while  
252 in the non-growing season, the decrease in irrigation water made the reservoir expand. In  
253 addition, the precipitation in the growing season was larger than that of the non-growing season,  
254 which led to a small increase in the reservoir area from August to September, as well as a small  
255 decrease in the distance between the observation point and reservoir (Figure 4b).



256

257 Figure 4. The interannual and seasonal variations in the Guanting Reservoir area and the distance between  
 258 the observation point (40 m tower) and the reservoir from 2013 to 2017: (a) interannual and (b) seasonal.

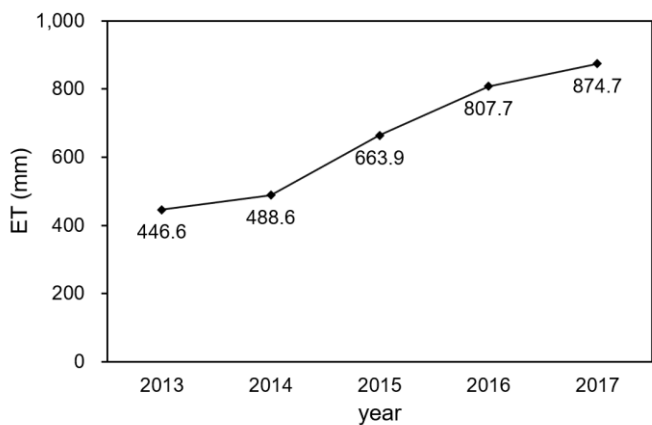
259 **3.2 Variations in Energy and Water Vapor Fluxes in the Surrounding Area of the**  
 260 **Reservoir**

261 The spatial scale of LAS measurement is kilometers, so this measurement can represent the  
 262 average conditions at the regional scale. The LAS of the Huailai Experiment Station is 14 m  
 263 high, and its path length is 1870 m. The 90% contribution source area of LAS has an average  
 264 length of approximately 2000 m and a width of approximately 850 m, and the average area is  
 265 approximately 1.7 km<sup>2</sup>. Therefore, the characteristics of the LAS observations were used to  
 266 represent the overall situation of water vapor and energy flux in the surrounding area of the  
 267 Guanting Reservoir. In addition, the 40 m tower was located in the center of the LAS source  
 268 area, so the meteorological elements observed by the 40 m tower can represent the  
 269 meteorological characteristics of the area surrounding the reservoir.

270 **3.2.1 The Variation in ET**

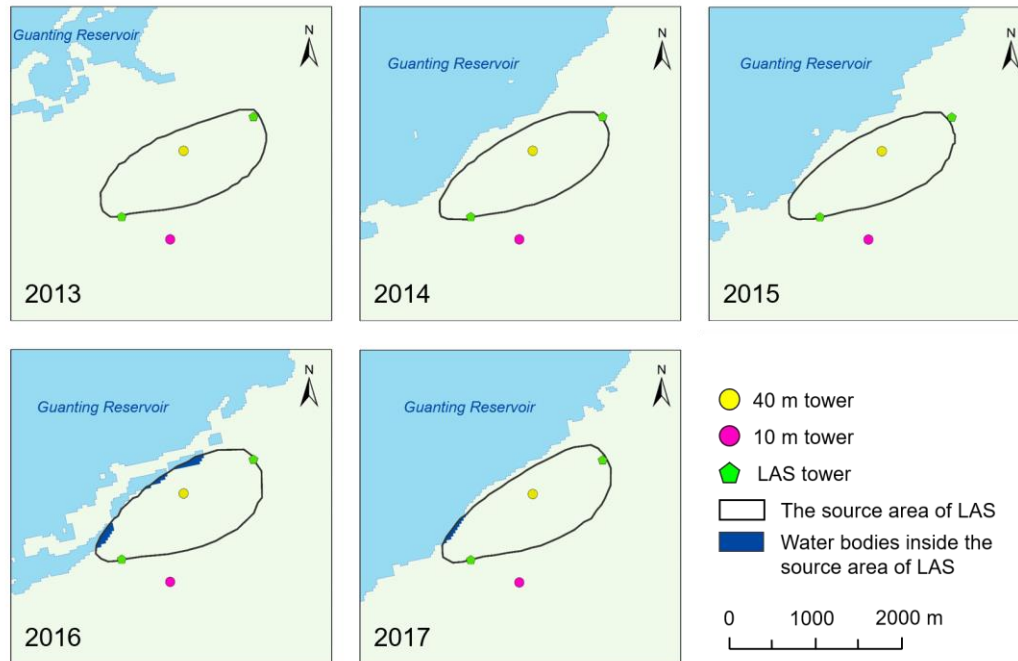
271 The annual cumulative ET of the surrounding area from 2013 to 2017 was obtained by the  
 272 daily ET data observed by LAS, and its variation is shown in Figure 5. From 2013-2017, the  
 273 annual average ET in the surrounding area was approximately 656.3 mm and increased year by

274 year along with the expansion of the Guanting Reservoir, from 446.6 mm in 2013 to 874.7 mm  
275 in 2017. In the area surrounding the Guanting Reservoir, ET was mainly affected by  
276 meteorological factors and underlying surface conditions, including the area ratio of water bodies  
277 in the LAS source area, vegetation factors and soil factors. The expansion and shrinkage of the  
278 reservoir would also affect ET by affecting the meteorological characteristics.



279  
280 Figure 5. The interannual variation in annual ET observed by LAS from 2013 to 2017.

281 Figure 6 shows the change in the 90% contribution source area of LAS during the growing  
282 season from 2013 to 2017. Along with the expansion of the reservoir, the distance between the  
283 source area and the reservoir decreased significantly. From 2013-2015, there was no water body  
284 in the LAS source area. Until 2016 and 2017, the reservoir expanded to the interior of the LAS  
285 source area, and the area ratio of the water body was approximately 3.18% in 2016 and 1.33% in  
286 2017 (Figure 6). The continuous expansion of the Guanting Reservoir changed the underlying  
287 surface of the LAS source area from a single farmland to a transition zone between water and  
288 farmland, increasing the proportion of water evaporation in the evapotranspiration (ET) of the  
289 source area. Therefore, the increase in the proportion of water bodies was the factor directly  
290 impacting on the increase in annual cumulative ET.



291

292

Figure 6. The interannual variation in annual ET observed by LAS from 2013 to 2017.

293

294

295

296

297

298

299

300

301

302

303

304

Figure 7 shows the seasonal variation in ET from 2013-2017. In one year, the ET first increased, reaching the maximum for the whole year in July-August, and then decreased to the minimum in winter. Comparing the seasonal variations in ET in each year, we can divide this changing regularity into three stages: [1] in spring (January to June), the ET of the surrounding area in 2014-2017 was significantly larger than that in 2013 and increased year by year. [2] In summer and autumn (July to September), there was no significant increase in ET, except in 2014. [3] In winter (October to December), the ET again shows an increasing trend year by year, but not as obvious as the first stage; however, the ET in 2014 was lower than that in 2013. In addition, in 2013, ET reached its peak in August, but since the expansion of the Guanting Reservoir in 2014, the peak appeared early in July, and the peak value of the monthly ET also increased from 119.5 mm in 2013 to 138.7 mm in 2017. These changes in the seasonal variation in ET were consistent with the seasonal changes in the reservoir (which are shown in Figure 4b).

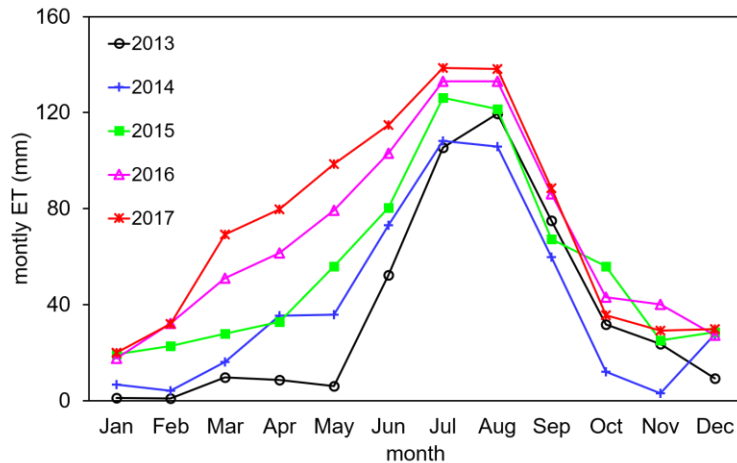


Figure 7. Seasonal variation in ET from 2013-2017.

305

306

307

308

309

310

311

312

313

314

315

316

317

318

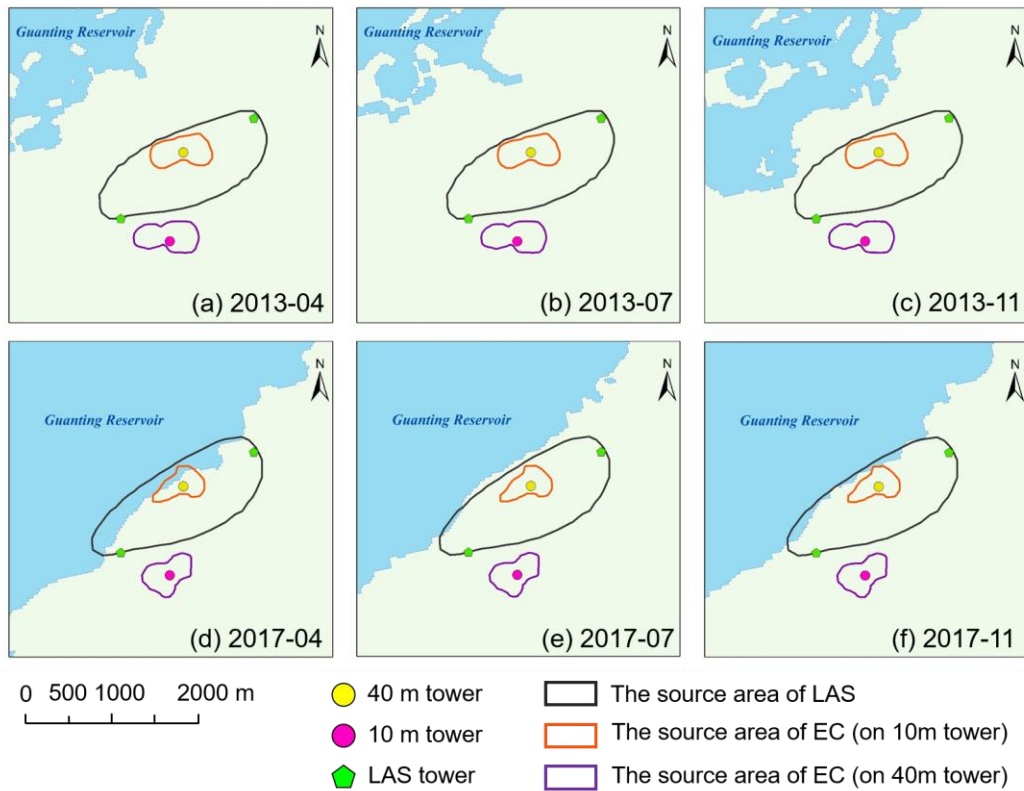
319

320

321

Figure 8 shows the 90% contribution source area of LAS during spring, summer/autumn and winter before and after the expansion, corresponding to the three stages of seasonal variation in ET. The proportion of water bodies varies in different seasons. Before reservoir expansion (taking 2013 as an example), there was no water body inside the source area (Figure 8a to c), but after expansion (taking 2017 as an example), the proportion of water bodies in the source area was higher in spring and winter and lower in summer and autumn. The water area ratio was approximately 25.67% in the spring of 2017 (Figure 8d), so water evaporation had a higher proportion of ET. At this time, maize had not yet emerged, so the ET of the land was mainly dominated by bare soil evaporation. In summer and autumn, seasonal shrinkage of the Guanting Reservoir occurred, and the area ratio of water bodies in the LAS source area decreased to approximately 1.33% (Figure 8e), so the proportion of water body evaporation was low in the LAS source area. At this time, the maize field was in its growing season, the crop transpiration was higher than bare soil evaporation, and the ET reached its peak. In the winter of 2017, the reservoir expanded again, but the expansion was not as obvious as that in the spring, and the water area ratio in the LAS source area increased to 6.67% until November (Figure 8f). Since the

322 maize had been cut, the bare soil evaporation took up a higher proportion of the ET of the  
 323 surrounding area. Therefore, from 2013 to 2017, the ET of the surrounding area of the Guanting  
 324 Reservoir increased in spring, remained almost unchanged in summer and autumn, and increased  
 325 again in winter.



326  
 327 Figure 8. The 90% contribution source areas of LAS and ECs: (a, d) during spring (April), (b, e) summer  
 328 (July) and (c, f) winter (November) in 2013 (before reservoir expansion) and 2017 (after expansion).

329 The expansion and shrinkage of the reservoir could also affect the energy and water vapor  
 330 fluxes by affecting meteorological factors and underlying surface conditions in the surrounding  
 331 area. In this study, net radiation ( $R_n$ ) and precipitation ( $P$ ) were considered to be the main  
 332 meteorological factors. The underlying surface conditions include vegetation and soil factors.  
 333 The average NDVI in the LAS source area was chosen to characterize vegetation growth

334 conditions, and surface and deep soil moisture ( $M_{S0-40\text{ cm}}$  and  $M_{S40-160\text{ cm}}$ ) represented the soil  
335 moisture conditions. The distance between the 40 m tower and reservoir (D) was also considered,  
336 which can reflect the expansion and shrinkage of the reservoir. D is the direct factor that affects  
337 ET, while meteorological and underlying surface factors are indirect factors. Since the ET in the  
338 surrounding area was dominated by crop transpiration in the growing season and by bare soil  
339 evaporation in the non-growing season, the main indirect factors affecting ET were different in  
340 those two periods. Therefore, in this study, we analyzed the correlation between the impact  
341 factors and monthly ET in both growing (May to September) and non-growing seasons (January  
342 to April, October to December). The results of the correlation analysis are displayed in Table 2  
343 and Table 3.

344 Table 2 shows the results of the correlation analysis during the growing seasons. Rn had the  
345 best significant correlation with monthly ET (the Pearson correlation coefficient was 0.735), so  
346 the monthly ET was most related to the energy factors in the growing season. There was also a  
347 positive correlation between monthly ET and deep soil moisture (the correlation coefficient was  
348 0.625), which was directly affected by the groundwater table caused by the seasonal expansion  
349 and shrinkage of the reservoir. Deep soil moisture was also related to vegetation conditions  
350 because maize could absorb deep soil moisture through its roots. Monthly ET had a positive  
351 correlation with NDVI (the correlation coefficient was 0.644). The vegetation growth condition  
352 was not only affected by agricultural activities but also controlled by net radiation and soil  
353 moisture. Therefore, during the growing season, the expansion and shrinkage of the reservoir has  
354 an indirect effect on ET by changing the net radiation, deep soil moisture and vegetation growth  
355 conditions.

356 Table 2. The correlation between impact factors and monthly ET during the growing season in 2013-2017

Monthly ET	D	Rn	P	NDVI	MS <sub>0-40 cm</sub>	MS <sub>40-160 cm</sub>
Pearson correlation	-0.319	.735**	.487*	.644**	0.258	.625**
Significance	0.12	0.000	0.014	0.001	0.213	0.001
N cases	25	23	25	25	25	25

*Note.* \* The correlation was significant at 0.05 level. \*\* The correlation was significant at 0.01 level.

357 In the non-growing season, the land had almost no vegetation, and the ET was mainly  
358 dominated by bare soil evaporation, so the influence of the NDVI factor was excluded from the  
359 correlation analysis. Table 3 shows the results of the correlation analysis during the non-growing  
360 season in 2013-2017. First, the monthly ET was significantly negatively correlated with the  
361 distance between the study area and reservoir, with a correlation coefficient of -0.693. This result  
362 means that during the non-growing season, reservoir expansion directly changed the proportion  
363 of water bodies in the LAS source area and became the main factor affecting ET in the  
364 surrounding area of the Guanting Reservoir. Second, the monthly ET was related to net radiation,  
365 which means that the monthly ET was also controlled by the available energy factor. In addition,  
366 ET also has a good correlation with surface soil moisture. In the non-growing season, the  
367 precipitation was low, and surface soil moisture became the major water source for bare soil  
368 evaporation. The surface soil moisture could directly affect bare soil evaporation, thus affecting  
369 ET in the non-growing season.

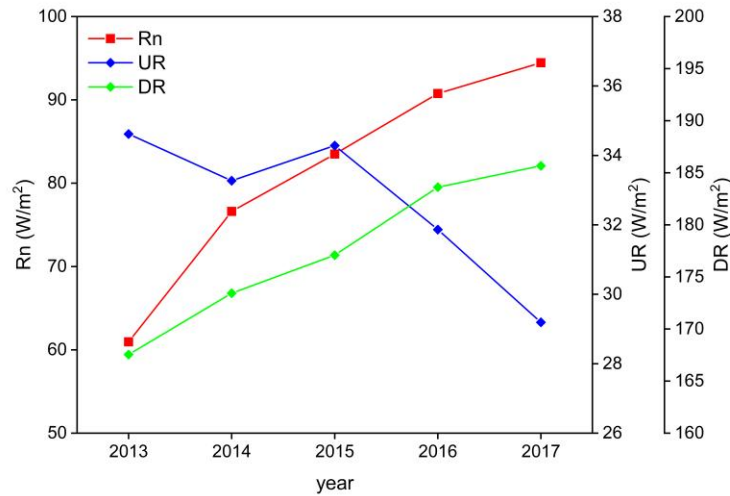
370 Table 3. The correlation between impact factors and monthly ET during the non-growing season in 2013-

371 2017

Monthly ET	D	Rn	P	MS <sub>0-40cm</sub>	MS <sub>40-160cm</sub>
Pearson correlation	-.693*	.641**	0.156	.530**	.424*

Significance	0.012	0.000	0.372	0.001	0.012
N cases	12	33	35	35	34

Note. \* The correlation was significant at 0.05 level. \*\* The correlation was significant at 0.01 level.



372

373 Figure 9. The variation in the net radiation (Rn) and upward shortwave radiation (UR) and downward  
 374 shortwave radiation (DR) at the 40 m tower from 2013 to 2017.

375 In both the growing and non-growing seasons, the monthly ET in the area surrounding the  
 376 Guanting Reservoir had a significant correlation with net radiation, soil moisture, and vegetation  
 377 conditions. On the one hand, the expansion of the reservoir increased the groundwater table and  
 378 then increased both surface and deep soil moisture. On the other hand, the increase in soil  
 379 moisture led to a decrease in albedo in the surrounding area, which decreased upward shortwave  
 380 radiation (UR). Meanwhile, the expansion of the reservoir also decreased the aerosols, which  
 381 increased the downward shortwave radiation (DR) (Figure 9). The decrease in upward radiation

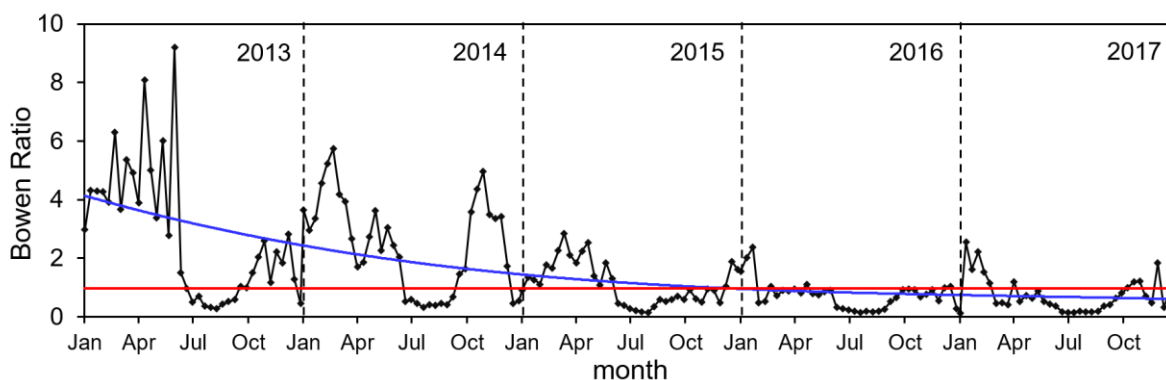
382 and the increase in downward radiation led to an increase in the net radiation ( $R_n$ ) in the  
383 surrounding area.

### 384 **3.2.2 The Variation in Bowen Ratio**

385 The Bowen ratio is the ratio of the sensible heat flux ( $H$ ) to the latent heat flux ( $LE$ ), which  
386 can reflect the partition of surface available energy. This ratio is also affected by environmental  
387 factors, including meteorological factors and the underlying surface conditions (such as  
388 vegetation growth conditions and soil moisture). Therefore, the Bowen ratio will also change  
389 with the interannual and seasonal expansion and shrinkage of lakes/reservoirs.

390 Using the  $H$  and  $LE$  data obtained by LAS, we calculated the Bowen ratio of the  
391 surrounding area of the Guanting Reservoir and then analyzed the characteristics of its  
392 interannual and seasonal variations. Figure 10 shows the variation in the Bowen ratio in the  
393 surrounding area from 2013 to 2017. In 2013 (before the expansion of the reservoir), the average  
394 Bowen ratio was approximately 2.7. Since 2014, with the expansion of the reservoir, the annual  
395 Bowen ratio has decreased year by year. Until 2016 and 2017, the Bowen ratio was almost less  
396 than 1 for the whole year and tended to be stable, and the average Bowen ratio was only  
397 approximately 0.75. In addition, in the non-growing season, the Bowen ratio was greater than 1,  
398 which means that  $H$  was larger than  $LE$ . During this period, the available surface energy was  
399 mainly consumed by turbulent heat exchange. In the growing season, the Bowen ratio was less  
400 than 1. Maize in the surrounding area of the Guanting Reservoir grew vigorously at this time,  
401 and the soil moisture and air temperature were high, so the incoming available surface energy  
402 was mainly consumed by evapotranspiration. In the growing season, the Bowen ratio did not  
403 obviously decrease from 2013 to 2017, but in the non-growing season, the Bowen ratio  
404 significantly decreased. This phenomenon was also related to the seasonal variation in the

405 reservoir. In the non-growing season, the proportion of water bodies in the LAS source area  
 406 increased significantly (Figure 8), resulting in an increase in the LE from 2013 to 2017, as well  
 407 as a decrease in the Bowen ratio. Therefore, with the expansion of the Guanting Reservoir, the  
 408 partition of available energy in its surrounding area tended toward ET.



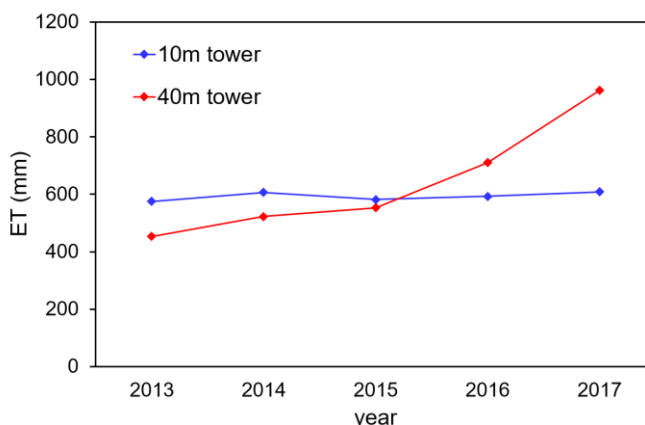
409  
 410 Figure 10. The variation in ten-day Bowen ratio from 2013 to 2017. The red line means the Bowen ratio  
 411 is 1, and the blue line shows the variation trend of the Bowen ratio.

412 **3.3 Variations in Energy and Water Vapor Fluxes at Different Distances from the**  
 413 **Guanting Reservoir**

414 In section 3.2, we analyzed the impact of the expansion and shrinkage of the Guanting  
 415 Reservoir on energy and water vapor fluxes in the surrounding area. However, for the areas at  
 416 different distances from the reservoir, this impact was also different. The Huailai Experiment  
 417 Station has two ECs located at the 10 m and 40 m towers. The 10 m tower was further from the  
 418 Guanting Reservoir, and the underlying surface in the EC source area was mainly irrigated maize  
 419 field. The 40 m tower was closer to the reservoir, and its underlying surface was mainly a non-  
 420 irrigated maize field. With the expansion of the reservoir, the distance between the 10 m tower  
 421 and the reservoir decreased from approximately 1600 m in 2013 to approximately 930 m in

422 2017, and the distance between the 40 m tower and the reservoir decreased from approximately  
423 720 m in 2013 to approximately 290 m in 2017.

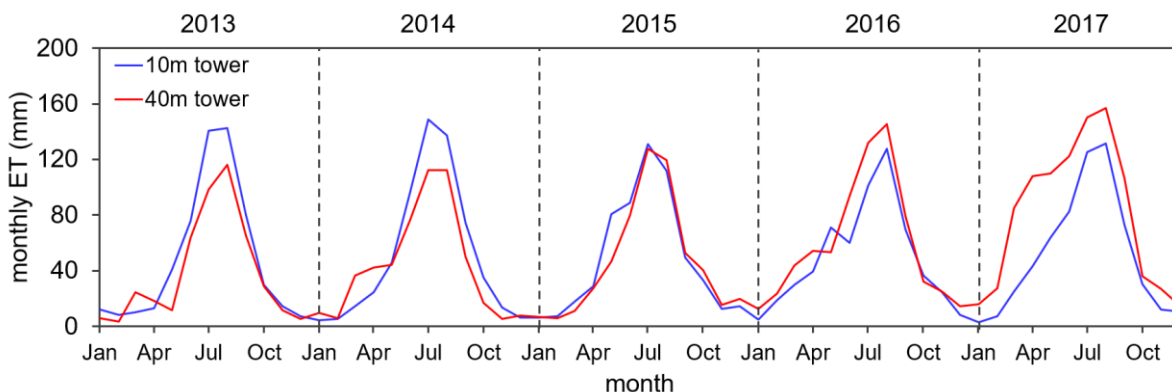
424 Figure 11 shows the variation in the annual ET at the 10 m and 40 m towers from 2013 to  
425 2017. With the expansion of the reservoir, the ET at the 10 m tower remained almost unchanged  
426 during the five years and was stable at approximately 593 mm, while the ET at the 40 m tower  
427 continued to increase year by year. Before 2015, the 10 m and 40 m towers were both far from  
428 the Guanting Reservoir. Since the 10 m tower was in an irrigated field, the ET at the 10 m tower  
429 was larger than the ET at the 40 m tower before 2015. With reservoir expansion and the increase  
430 in ET at the 40 m tower, after 2015, the ET at the 40 m tower became larger than the ET at the  
431 10 m tower.



432  
433 Figure 11. The variation in the annual ET at the 10 m and 40 m towers from 2013 to 2017.

434 The seasonal variation in ET at the 10 m and 40 m towers is shown in Figure 12. The ET at  
435 the 10 m and 40 m towers reached a peak almost at the same time in each year (in July to  
436 August), but their peak values were different. The peak value of ET at the 10 m tower in 2015-  
437 2017 was lower than that in 2013-2014, but the peak value of ET at the 40 m tower increased  
438 year by year from 2015 to 2017. Since the 10 m tower was in the irrigated field, in the growing

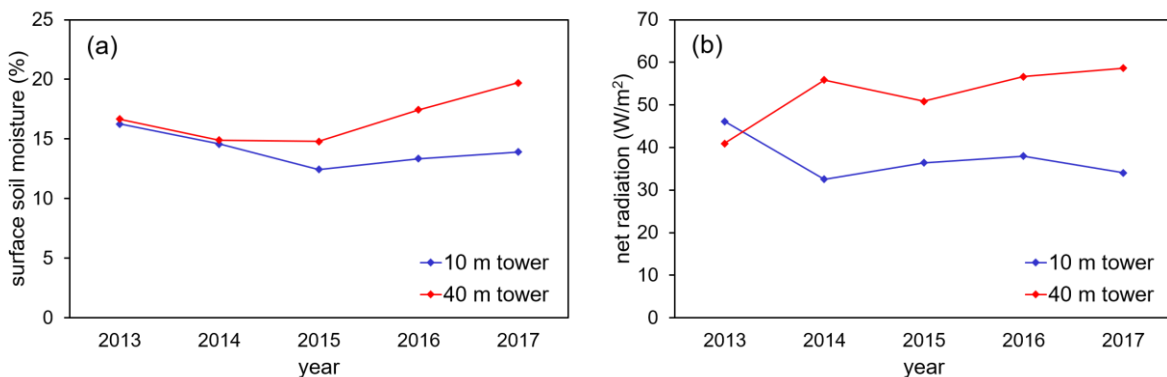
439 season (May-September) of 2013-2015, the ET at the 10 m tower was larger than that of the 40  
 440 m tower. With the reservoir expanding year by year, the ET at the 40 m tower was more affected  
 441 by the expansion and led to the increase in the peak value of ET at the 40 m tower.



442  
 443 Figure 12. The seasonal variation in ET at the 10 m and 40 m towers from 2013 to 2017.

444 During the growing season, the reservoir has seasonal shrinkage, and there were no water  
 445 bodies in the EC source areas of both the 10 m and 40 m towers (Figure 8b, e), so the ET at the  
 446 40 m tower was not significantly different from that at the 10 m tower in 2013-2017. During the  
 447 non-growing season (January-April, October-December), the reservoir experiences seasonal  
 448 expansion, and the ET values at the 10 m and 40 m towers were similar to each other in 2013 and  
 449 2014, but since 2015, the difference between the ET values at the two sites increased. This  
 450 difference was more obvious in spring because the seasonal expansion in spring was more  
 451 obvious than that in winter. On the one hand, the proportion of water bodies in the EC source  
 452 area at the 40 m tower increased rapidly after reservoir expansion (for example, the water area  
 453 ratio was approximately 20.42% in spring 2017, Figure 8d, f), which directly led to the increase  
 454 in ET at the 40 m tower site. However, there was no water body in the EC source area at the 10  
 455 m tower in 2013-2017. On the other hand, because of reservoir expansion, the surface soil  
 456 moisture at the 40 m tower site had a larger growth rate than that of the 10 m tower site, which is

457 shown in Figure 13a. Figure 13b indicates that the increase in net radiation was obvious at the 40  
 458 m tower, while the net radiation at the 10 m tower did not increase. Since bare soil evaporation  
 459 was the major component of ET during the non-growing season, the increase in surface soil  
 460 moisture was another factor affecting the increase in ET at the 40 m tower, and the increasing net  
 461 radiation provided more available energy to increase ET.



462  
 463 Figure 13. The seasonal variation in ET at the 10 m and 40 m towers from 2013 to 2017.

464 **4. Conclusions**

465 In this study, remote sensing data were used to analyze the expansion and shrinkage of the  
 466 Guanting Reservoir, and LAS, EC and AWS data from the Huailai Experiment Station were used  
 467 to study the variation characteristics of energy and water vapor fluxes in the surrounding area, as  
 468 well as their relationships with the expansion and shrinkage of the reservoir. The main findings  
 469 of this study are as follows: [1] The area of the Guanting Reservoir increased year by year from  
 470 2013-2017, and the distance between the study area and the reservoir gradually decreased year  
 471 by year. The seasonal variation in the Guanting Reservoir was characterized by expansion in  
 472 spring, shrinkage in summer and autumn, and expansion again in winter within one year. [2] In  
 473 the surrounding area of the reservoir, the ET increased year by year with the expansion of the  
 474 Guanting Reservoir and had a seasonal variation that was affected by the seasonal expansion and

475 shrinkage of the reservoir by changing the proportion of water bodies in the source area, net  
476 radiation and soil moisture. In the growing season, the seasonal shrinkage of the reservoir has an  
477 indirect effect on ET by changing the net radiation, deep soil moisture and vegetation growth  
478 conditions, while in the non-growing season, the seasonal expansion of the reservoir increased  
479 the proportion of the water body in the LAS source area, which was the direct factor affecting  
480 monthly ET, and the increase in Rn and soil moisture was also an important factor that affected  
481 ET. The partition of available energy in the reservoir's surrounding area tended toward ET with  
482 reservoir expansion. [3] In the surrounding area with different distances from the reservoir, the  
483 difference in ET between at the closer site and further site from the reservoir increased  
484 obviously, especially in the non-growing season. The expansion and shrinkage of the reservoir  
485 had a greater impact on the surrounding areas closer to the reservoir.

486 In this study, part of the remote sensing data acquired has problems such as being covered  
487 by clouds, which are more common in summer (growing season), and therefore, only the images  
488 with the most appropriate times and high quality could be selected in the study, which brings  
489 great uncertainty to the analysis.

#### 490 **Acknowledgments**

491 This work was supported by the National Key Research & Development Program of China  
492 (2016YFC0500101) and the National Natural Science Foundation of China (41771364). The  
493 ground-measured turbulent heat fluxes and meteorological variables were obtained from  
494 National Tibetan Plateau Data Center (<http://data.tpdc.ac.cn>). Landsat OLI (Operational Land  
495 Imager) data were downloaded from the United States Geological Survey (USGS) website  
496 (<https://earthexplorer.usgs.gov/>).

497 **References**

- 498 Ao, Y. H., Lv, S. H., Han, B., & Li, Z. G. (2013). Analysis on micrometeorology characteristics in surface layer  
499 over Badan Jaran Desert in summer. *Plateau Meteorology*, 32(6), 1682-1691. (in Chinese, abstract in English)
- 500 Bates, G. T., Giorgi, F., & Hostetler, S. W. (1993). Toward the simulation of the effects of the Great Lakes on  
501 regional climate. *Monthly Weather Review*, 121, 1373-1387. [https://doi.org/10.1175/1520-0493\(1993\)121<1373:TTSOTE>2.0.CO;2](https://doi.org/10.1175/1520-0493(1993)121<1373:TTSOTE>2.0.CO;2)
- 503 Biermann, T., Babel, W., Ma, W. Q., Chen, X. L., Thiem, E., Ma, Y. M., & Folken, T. (2014). Turbulent flux  
504 observations and modelling over a shallow lake and a wet grassland in the Nam Co basin, Tibetan Plateau.  
505 *THEORETICAL AND APPLIED CLIMATOLOGY*, 116(1-2), 301-316. [https://doi.org/10.1007/s00704-013-0953-](https://doi.org/10.1007/s00704-013-0953-6)  
506 6
- 507 Chen, Y. P. (2007). Present situation analysis of water resources in Guanting Reservoir. *Beijing Water*, 6, 7-11. (in  
508 Chinese, abstract in English)
- 509 Downing, J., Prairie, Y., Cole, J., Duarte, C., Tranvik, L., Striegl, R., et al. (2006). The Global Abundance and Size  
510 Distribution of Lakes, Ponds, and Impoundments. *Limnology and Oceanography*, 51(5), 2388-2397.  
511 <https://doi.org/10.4319/lo.2006.51.5.2388>
- 512 Guo, H., Hu, Q., & Jiang, T. (2008). Annual and seasonal streamflow responses to climate and land-cover changes  
513 in the Poyang Lake basin, China. *Journal of Hydrology*, 355(1-4), 106-122.  
514 <https://doi.org/10.1016/j.jhydrol.2008.03.020>
- 515 Guo, H., Hu, Q., Zhang, Q., & Feng, S. (2012). Effects of the Three Gorges Dam on Yangtze River flow and river  
516 interaction with Poyang Lake, China: 2003-2008. *Journal of Hydrology*, 416-417, 19-27.  
517 <https://doi.org/10.1016/j.jhydrol.2011.11.027>
- 518 Haddeland, I., Heinke, J., Biemans, H., Eisner, S., Flörke, M., Hanasaki, N., et al. (2014). Global water resources  
519 affected by human interventions and climate change. *Proceedings of the National Academy of Sciences*, 111(9),  
520 3251-3256. <https://doi.org/10.1073/pnas.1222475110>

521 He, H. W., Zhu, Y. J., and He, C. C. (2013). Hebei Friendship Reservoir transfers water to Beijing Guanting  
522 Reservoir, plans to release water for 12 days, Accessed 9 October 2013,  
523 <http://report.hebei.com.cn/system/2013/10/09/013010597.shtml>. (in Chinese)

524 Jia, Z. Z., Liu, S. M., Xu, Z. W., Chen, Y. J., & Zhu, M. J. (2012). Validation of remotely sensed evapotranspiration  
525 over the Hai River Basin, China. *Journal of Geophysical Research: Atmospheres*, *117*, 13113.  
526 <https://doi.org/10.1029/2011JD017037>

527 Kodama, Y., Eaton, F., & Wendler, G. (1983). The Influence of Lake Minchumina, Interior Alaska, on Its  
528 Surroundings. *Archives for Meteorology, Geophysics, and Bioclimatology Series B*, *33*, 199-218.  
529 <https://doi.org/10.1007/BF02275094>

530 Kormann, R., & Meixner, F. X. (2001). An analytic footprint model for neutral stratification. *Boundary-Layer*  
531 *Meteorology*, *99*(2), 207-224. <https://doi.org/10.1023/A:1018991015119>

532 Lee, X. H., Liu, S. D., Xiao, W., Wang, W., Gao, Z. Q., Cao, C., et al. (2014). The Taihu Eddy Flux Network: An  
533 Observational Program on Energy, Water, and Greenhouse Gas Fluxes of a Large Freshwater Lake. *Bulletin of the*  
534 *American Meteorological Society*, *95*(10), 1583-1594. <https://doi.org/10.1175/BAMS-D-13-00136.1>

535 Li, X. Y., Ma, Y. J., Huang, Y., Hu, X., Wu, X. C., Wang, P., et al. (2016). Evaporation and surface energy budget  
536 over the largest high-altitude saline lake on the Qinghai-Tibet Plateau. *Journal of Geophysical Research:*  
537 *Atmospheres*, *121*, 10470-10485. <https://doi.org/10.1002/2016JD025027>

538 Li, X., Liu, S., Li, H., Ma, Y., Wang, J., Zhang, Y., et al. (2018). Intercomparison of six upscaling  
539 evapotranspiration methods: From site to the satellite pixel. *Journal of Geophysical Research: Atmospheres*, *123*,  
540 6777-6803. <https://doi.org/10.1029/2018JD028422>

541 Liebethal, C., Huwe, B., & Foken, T. (2005). Sensitivity analysis for two ground heat flux calculation approaches.  
542 *Agricultural and Forest Meteorology*, *132*(3-4), 253-262. <https://doi.org/10.1016/j.agrformet.2005.08.001>

543 Liu, H. P., Zhang, Q. Y., & Dowler, G. (2012). Environmental Controls on the Surface Energy Budget over a Large  
544 Southern Inland Water in the United States: An Analysis of One-Year Eddy Covariance Flux Data. *Journal of*  
545 *Hydrometeorology*, *13*(6), 1893-1910. <https://doi.org/10.1175/JHM-D-12-020.1>

546 Liu, S. M., Xu, Z. W., Wang, W. Z., Jia, Z. Z., Zhu, M. J., Bai, J., & Wang, J. M. (2011). A comparison of eddy-  
547 covariance and large aperture scintillometer measurements with respect to the energy balance closure problem.  
548 *Hydrology and Earth System Sciences*, 15, 1291-1306. <https://doi.org/10.5194/hess-15-1291-2011>

549 Liu, S. M., Xu, Z. W., Zhu, Z. L., Jia, Z. Z., & Zhu, M. J. (2013). Measurements of evapotranspiration from eddy-  
550 covariance systems and large aperture scintillometers in the Hai River Basin, China. *Journal of Hydrology*, 487,  
551 24-38. <https://doi.org/10.1016/j.jhydrol.2013.02.025>

552 Liu, S. M., Xu, Z. W., Song, L. S., Zhao, Q. Y., Ge, Y., Xu, T. R., et al. (2016). Upscaling evapotranspiration  
553 measurements from multi-site to the satellite pixel scale over heterogeneous land surfaces. *Agricultural and*  
554 *Forest Meteorology*, 230-231, 97-113. <https://doi.org/10.1016/j.agrformet.2016.04.008>

555 Liu, X. M., Hu, F., Jiang, J. H., & Zhen, C. M. (2008). Energy budget over the water-land heterogeneous surface in  
556 Baiyangdian Region. *Chinese Journal of Atmospheric Sciences*, 32(6), 1411-1418. (in Chinese, abstract in  
557 English)

558 Ma, D., Lv, S. H., Ao, Y. H., and Lin, Z. (2012). Analyses on radiation balance and surface energy budget in the  
559 Badain Jaran Desert in summer. *Plateau Meteorology*, 31, 615-621. (in Chinese, abstract in English)

560 Ma, Z. G., Li, L. L., & Zhang, L. Y. (2014). Analysis of water area changes of Guanting reservoir and related factors  
561 from 1978 to 2013. *Journal of Tianjin Normal University (Natural Science Edition)*, 34(2), 56-60. (in Chinese,  
562 abstract in English)

563 Min, Q. (1995). On the regularities of water level fluctuations in Poyang Lake, *Journal of Lake Sciences*, 7(3), 281-  
564 288. (in Chinese, abstract in English)

565 Nordbo, A., Launiainen, S., Mammarella, I., Leppäranta, M., Huotari, J., Ojala, A., & Vesala, T. (2011). Long-term  
566 energy flux measurements and energy balance over a small boreal lake using eddy covariance technique. *Journal*  
567 *of Geophysical Research: Atmospheres*, 116, D02119. <https://doi.org/10.1029/2010JD014542>

568 Rouse, W. R., Oswald, C. J., Binyamin, J., Spence, C., Schertzer, W. M., Blanken, P. D., Bussi eres, N., & Duguay,  
569 C. R. (2005). The role of northern lakes in a regional energy balance, *Journal of Hydrometeorology*, 6, 291-305.  
570 <https://doi.org/10.1175/JHM421.1>

571 Ruan, R. Z., Xia, S., Chen, Y., She, Y. J., & Yan, M. C. (2012). Change of lake nearby Linhuai Town in west bank  
572 of Hongze Lake during 1979-2006. *Wetland Sciences*, 10(3), 344-349. (in Chinese, abstract in English)

573 Shadkam, S., Ludwig, F., van Vliet, M. T. H., Pastor, A., & Kabat, P. (2016). Preserving the world second largest  
574 hypersaline lake under future irrigation and climate change. *Science of The Total Environment*, 559, 317-325.  
575 <https://doi.org/10.1016/j.scitotenv.2016.03.190>

576 Shi, X., Xiao, W. H., Wang, Y., & Wang, X. (2012). Characteristics and factors of water level variations in the  
577 Dongting Lake during the recent 50 year. *South-to-North Water Diversion and Water Science & Technology*, 5,  
578 18-22. (in Chinese, abstract in English)

579 Venäläinen, A., Heikinheimo, M., & Tourula, T. (1998). Latent heat flux from small sheltered lakes, *Boundary-*  
580 *Layer Meteorology*, 86, 355-377. <https://doi.org/10.1023/A:1000664615657>

581 Vesala, T., Huotari, J., Rannik, Ü., Suni, T., Smolander, S., Sogachey, A., et al. (2006). Eddy covariance  
582 measurements of carbon exchange and latent and sensible heat fluxes over a boreal lake for a full open-water  
583 period. *Journal of Geophysical Research*, 111, D11101. <https://doi.org/10.1029/2005JD006365>

584 Wang, T., Ochs, G. R., & Clifford, S. F. (1978). Saturation-resistant optical scintillometer to measure  $C_n^2$ . *Journal*  
585 *of the Optical Society of America*, 68(3), 334–338. <https://doi.org/10.1364/JOSA.68.000334>

586 Wang, W., Shen, S. H., Liu, S. D., Zhang, M., Xiao, W., Wang, Y. W., & Lee, X. H. (2017). Mechanistic analysis of  
587 the observed energy imbalance of Lake Taihu. *Acta Ecologica Sinica*, 37(18), 5935-5950. (in Chinese, abstract in  
588 English)

589 Williamson, C. E., Saros, J. E., & Schindler, D. W. (2009). Sentinels of change. *Science*, 323(5916), 887-888.  
590 <https://doi.org/10.1126/science.1169443>

591 Xiao, K., Griffis, T., Baker, J., Bolstad, P., Erickson, M., Lee, X. H., et al. (2018). Evaporation from a temperate  
592 closed-basin lake and its impact on present, past, and future water level. *Journal of Hydrology*, 561, 59-75.  
593 <https://doi.org/10.1016/j.jhydrol.2018.03.059>

594 Xie, C., Huang, X., Mu, H. Q., & Yin, W. (2017). Impacts of Land-Use Changes on the Lakes across the Yangtze  
595 Floodplain in China. *Environmental Science & Technology*, 51, 3669–3677.  
596 <https://doi.org/10.1021/acs.est.6b04260>

- 597 Xu, Z. W., Liu, S. M., Li, X., Shi, S. J., Wang, J. M., Zhu, Z. L., et al. (2013). Intercomparison of surface energy  
598 flux measurement systems used during the HiWATER-MUSOEXE. *Journal of Geophysical Research:  
599 Atmospheres*, 118(23), 13140-13157. <https://doi.org/10.1002/2013JD020260>
- 600 Yang, J. M., & Zhang, Y. W. (2016). Thoughts on water source protection of Guanting Reservoir under the  
601 coordinated development of Beijing, Tianjin and Hebei. *Beijing Water*, 1, 48-50. (in Chinese)
- 602 Yang, Z., Cheng, C., Tan, X., Cheng, R., & Ma, Z. (2015). Analysis of water environmental capacity of Guanting  
603 Reservoir and its upstream basin. *Journal of Arid Land Resources and Environment*, 29(1), 163-168. (in Chinese,  
604 abstract in English)
- 605 Zhang, K. C., Ao, Y. H., Qu, J. J., An, Z. S., Zu, R. P., & Han, Q. J. (2014). Influences of lake-sand dune landscape  
606 on local microclimate in Badain Jaran Desert. *Bulletin of Soil and Water Conservation*, 34(5), 104-108. (in  
607 Chinese, abstract in English)